Korean J. Chem. Eng., 36(7), 1124-1130 (2019)
DOI: 10.1007/s11814-019-0289-8

pISSN: 0256-1115
eISSN: 1975-7220

Effects of air gap on membrane substrate properties and membrane performance for biomass processing

Elfira Anuar, Syed Mohd Saufi†, and Hafizuddin Wan Yussof

Faculty of Chemical and Natural Resources Engineering, Universiti Malaysia Pahang, Lebuhraya Tun Razak, 26300 Gambang, Pahang, Malaysia

(*Received 4 December 2018 • accepted 28 April 2019*)

Abstract−We studied a correlation between the membrane substrate properties and the final performance of hollow fiber thin film composite (TFC) membrane for xylose/glucose concentration and acetic acid removal. Polysulfone (PSf) hollow fiber membrane substrate was fabricated using 20 wt% PSf, 2 wt% polyvinylpyrrolidone and 78 wt% dimethylformamide via dry-wet spinning process. The air gap distance was manipulated from 6 cm to 15 cm during spinning to produce different substrate membrane properties. The molecular weight cut-off (MWCO) and porosity of the membrane substrate increased as the air gap distance increased. Membrane substrate that was spun at 6 cm air gap showed a rapid phase inversion without much chain relaxation, thus producing the smallest MWCO (8 kDa) and an average pore diameter (4.46 nm). The TFC membrane produced using this membrane substrate showed the best performance in terms of solute rejection and separation factor. The rejection for xylose, glucose and acetic acid was 91.66±0.09%, 67.28±13.97%, and 13.08±3.00%, respectively. This results in an ideal separation factor of 3.20±1.27 for acetic acid/glucose and 10.42±0.25 for acetic acid/xylose.

Keywords: Biorefinery, Sugar Separation, Hollow Fiber, Air Gap, Thin Film Composite Membrane

INTRODUCTION

Various types of membrane process have been developed and successfully applied at the industrial stage. Among them, nanofiltration (NF) and reverse osmosis (RO) are found suitable to be used in the biorefinery industry for sugar concentration, sugar separation and detoxification during biomass hydrolysate processing [1,2]. NF and RO membranes are commonly manufactured through surface modification on the membrane substrate via the interfacial polymerization (IP). An organic monomer is reacted with aqueous monomer in the IP process to form an active skin layer on the membrane substrate. This kind of membrane is called thin film composite (TFC) layer. Compared to the typical asymmetric NF or RO hollow fiber membranes, the selectivity and productivity of the TFC membranes are much better due to the fine adjustment of the membrane active skin structure.

Commercial, or ready-made hollow fiber ultrafiltration membrane, is normally used as a membrane substrate in TFC membrane preparation. Most studies are focusing on the optimization of IP process parameters to enhance the properties and performance of the TFC membrane [3,4]. However, only few studies have been reported on the correlation between hollow fiber membrane substrate to the final performance of the TFC membranes [5,6]. The selection of membrane substrate for the fabrication of defect-free and high-performance TFC layer must be taken seriously. The mechanical properties, morphology and performance of the hollow fiber membrane substrate can be optimized through spinning process parameters such as dope extrusion rate, type and flow rate of bore fluid, air gap distance, coagulant condition, spinneret design, and temperature.

The air gap plays a crucial role on the membrane morphology, mechanical strength and separation performance. Several researchers have investigated the relationship between hollow fiber membrane properties with the air gap length [7-9]. Long air gap can produce small pore size in the inner side of the hollow fiber membrane [10]. Khayet [11] reported that pure water permeation (PWP) flux of the polyvinylidene fluoride hollow fiber membrane had decreased and solute separation had increased when the air gap distance was increased. This is also due to the decrease in the membrane pore size. However, in another study, the pore size of the outer surface of the hollow fiber membrane increased as the air gap increased [12]. Chung et al. [13] observed that the number of defects on the external skin of the hollow fiber membrane increased as the air gap length increased. The tensile strength and the elongation at break of the membrane were affected by these defects. The studies clearly show that air gap distance plays a crucial part on the hollow fiber morphology and performance. In addition, the air gap distance can be easily manipulated during the dry-wet spinning process to prepare different properties of membrane substrates to be used during TFC membrane fabrication.

In the present study, a correlation between the membrane substrate properties and the final performance of the TFC hollow fiber membrane was studied. In developing different PSf hollow fiber membrane substrates, air gap distance was manipulated during the spinning process. IP was performed by using m-phenylenediamine (MPD) and trimesoyl chloride (TMC) monomers on the inner side of the hollow fiber membrane. The main innovative aspect of this

†To whom correspondence should be addressed.
E-mail: smsaufi@ump.edu.my

work is the fabrication of tailor-made TFC hollow fiber membrane for specific uses in a biorefinery. The effect of the membrane substrate to the final TFC performance has not been fully studied due to the use of the commercial or ready-made membrane substrate. Good membrane substrate is required in order to form a defect-free skin layer in the TFC membrane and to provide adequate mechanical strength during the filtration process. Hence, it is crucial to select the best membrane substrate to produce high performance TFC hollow fiber membrane for xylose/glucose concentration and acetic acid removal during biomass processing.

METHODS

1. Materials

Polysulfone (PSf, Udel P-3500) supplied by Solvay was used as polymer, polyvinylpyrrolidone (PVP K30) supplied by Sigma-Aldrich was used as the additive, and dimethylformamide (DMF) supplied by Merck was used as the solvent. n-Hexane purchased from Fisher Scientific, TMC purchased from Sigma-Aldrich and MPD purchased from Merck were used in the IP process. A performance test of the TFC membranes was conducted using xylose (Sigma-Aldrich), glucose (Sigma-Aldrich) and acetic acid (Fisher Scientific). In the molecular weight cut-off (MWCO) experiment, polyethylene glycol (PEG) with molecular weights of 1 kDa, 3 kDa, 10 kDa, 20 kDa, 35 kDa; and polyethyleneoxide (PEO) with a molecular weight of 100 kDa purchased from Merck were used. Pure water from Millipore Elix® 5 UV Water Purification System was used for the PWP measurement of the membranes.

2. Hollow Fiber Membrane Substrate Preparation

A dope solution with a mass ratio of 20% PSf/2% PVP K30/78% DMF was prepared [14]. The hollow fiber membrane was fabricated through dry-wet spinning process by using water at room temperature as the bore fluid and external coagulant. The inside and outside diameter of the spinneret was 2.0 mm and 2.6 mm, respectively. The dope and bore fluid flowrate was 18 mL/min and 150 mL/min, respectively. The air gap was varied at 6, 9, 12, and 15 cm, while other parameters were kept constant. The take-up speed was adjusted accordingly based on the air gap used to avoid fiber breakage during spinning. The hollow fiber membranes were kept in water for 72 hours at room temperature to remove the residual solvent. The fibers were then immersed in aqueous glycerol solution (10 wt%) for 24 hours and dried at room temperature for 7 days. For hollow fiber membrane module construction, the method proposed by Li et al. [15] was used. Five fibers with 30 cm long were selected and used in the module.

3. Interfacial Polymerization

The IP condition was adapted from the established method by Maurya et al. [14]. Before performing IP, the glycerol in the membranes pores was flushed with pure water for 30 minutes. 2.0 wt% of MPD was flowed to the lumen side of the fiber for 40 seconds, followed by nitrogen purging to remove excess monomer. To form a thin film, 0.1 wt% of TMC in hexane solution was then reacted for 40 seconds. The TFC membranes were cured in an oven at 60 °C for 3 minutes.

4. Cross-flow Filtration

The water flux, J_w (L/m^2·h) of the membranes was measured in cross-flow system using three different pressures of 1, 2 and 3 bar. Eq. (1) was used to compute the water flux. The value of slope in the plot of water flux versus pressure is corresponding to the PWP value.

$$J_w = \frac{\Delta V}{A \Delta t} \tag{1}$$

where ΔV, A and Δt are denoted as volume of permeate collected (L), effective membrane surface area (m^2) and sampling time of permeate (h), respectively.

Single feed solution of glucose, xylose, and acetic acid was used in the membrane performance test. Three liters of feed solution with 10 g/L concentration was used in each experiment. The cross-flow was conducted at 3 bar by circulating retentate stream back to the feed tank for 1 hour. The permeate flux was then measured using Eq. (1); the solute concentration in the permeate was analyzed; the rejection and separation factors were calculated using Eq. (2) and Eq. (3), respectively [2].

$$R(\%) = \left(1 - \frac{C_p}{C_f}\right) \times 100 \tag{2}$$

$$X_{s1/s2} = \frac{C_{p(s1)}/C_{p(s2)}}{C_{f(s1)}/C_{f(s2)}} \tag{3}$$

where R, C_p, C_f, s1, s2, and $X_{s1/s2}$ are the rejection of solute (%), solute concentration in permeate, solute concentration in feed solutions, solute 1, solute 2, and separation factor of solute 1 to solute 2, respectively.

5. Sample Analysis

Xylose and glucose concentration were analyzed using 3,5-dinitrosalicylic acid (DNS) method [16]. The acetic acid concentration was determined using HPLC column (Phenomenex Synergi 4U Hydro-RP 80A) with UV detection at wavelength of 211 nm as described previously [17].

6. Molecular Weight Cut-off (MWCO)

MWCO of the membrane was computed based on the PEG rejection data. The rejection was determined by running the cross-flow filtration using mixed PEG solutions (PEG 1 kDa to PEG 35 kDa) and single PEO 100 kDa. Eq. (2) was used to calculate the rejection value. The concentration of the PEG 1 kDa to PEG 35 kDa samples was analyzed using GFC column (Phenomenex PolySep-GFC-P4000; 300×7.8 mm). Meanwhile, the concentrations of the PEO 100 kDa samples were analyzed using the calorimetric method by measuring the absorbance at wavelength of 535 nm using UV-Vis spectrophotometer. The calorimetric reagent was prepared according to Yusoff et al. [18]. MWCO value was determined based on 90% solute rejection in the plot of rejection versus PEG/PEO molecular weight.

7. Porosity and Pore Size Calculation

The porosity of the membrane was determined based of the void fraction of the wet membrane after drying process as described previously [17]. The mean pore radius (r_m) of the membrane was calculated using Guerout-Elford-Ferry equation (Eq. (4)) based on porosity and pure water flux data at 3 bar.

$$r_m = \sqrt{\frac{(2.9 - 1.75\varepsilon) \times 8\mu l Q}{\varepsilon A \Delta P}} \tag{4}$$

where, μ is viscosity of the water (8.9×10^{-4} Pa s), Q is water flow rate (m^3/s) and ΔP is operating pressure (Pa).

RESULTS AND DISCUSSION

1. Molecular Weight Cut-off

The MWCO of the membrane substrate prepared at different air gap is demonstrated in Fig. 1. The MWCO was calculated based on 90% solute rejection. The MWCO of the membrane substrate increased as the air gap increased. The membrane substrates MWCO were 8 kDa, 24 kDa, 56 kDa, and 86 kDa for the membrane spun at 6-cm, 9-cm, 12-cm, and 15-cm air gap, respectively. The water vapor from the air acted as non-solvent additives to the dope solution. The amount of the water vapor penetrated into the polymer dope increased when the air gap increased, thus producing more porous structure. Apart from that, the stretch of fiber in the flow of spinning direction was increased at high air gap, which made the fiber thinner and produced large pores.

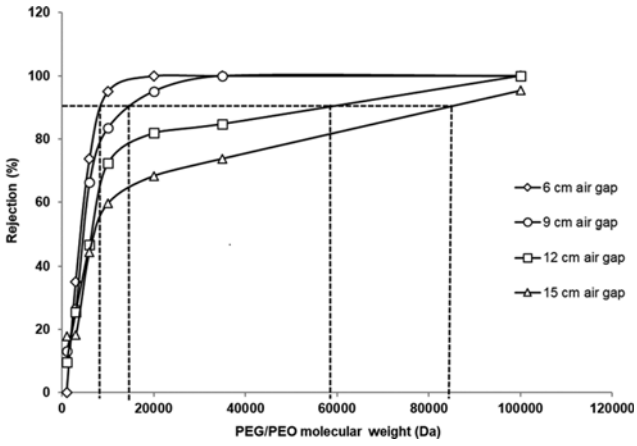

Fig. 1. MWCO of membrane substrate at different air gap lengths.

2. Membrane Morphology

Fig. 2 shows the cross-section and surface morphology of hollow fibers membrane substrate prepared at air gap lengths of 6 cm to 15 cm. It was proven that the air gap length greatly affected the structure of the hollow fiber membranes. As shown in Fig. 2, all spun fibers have needle-like pores underneath the inner and outer skin of the hollow fiber membranes. The inner finger-like macro-

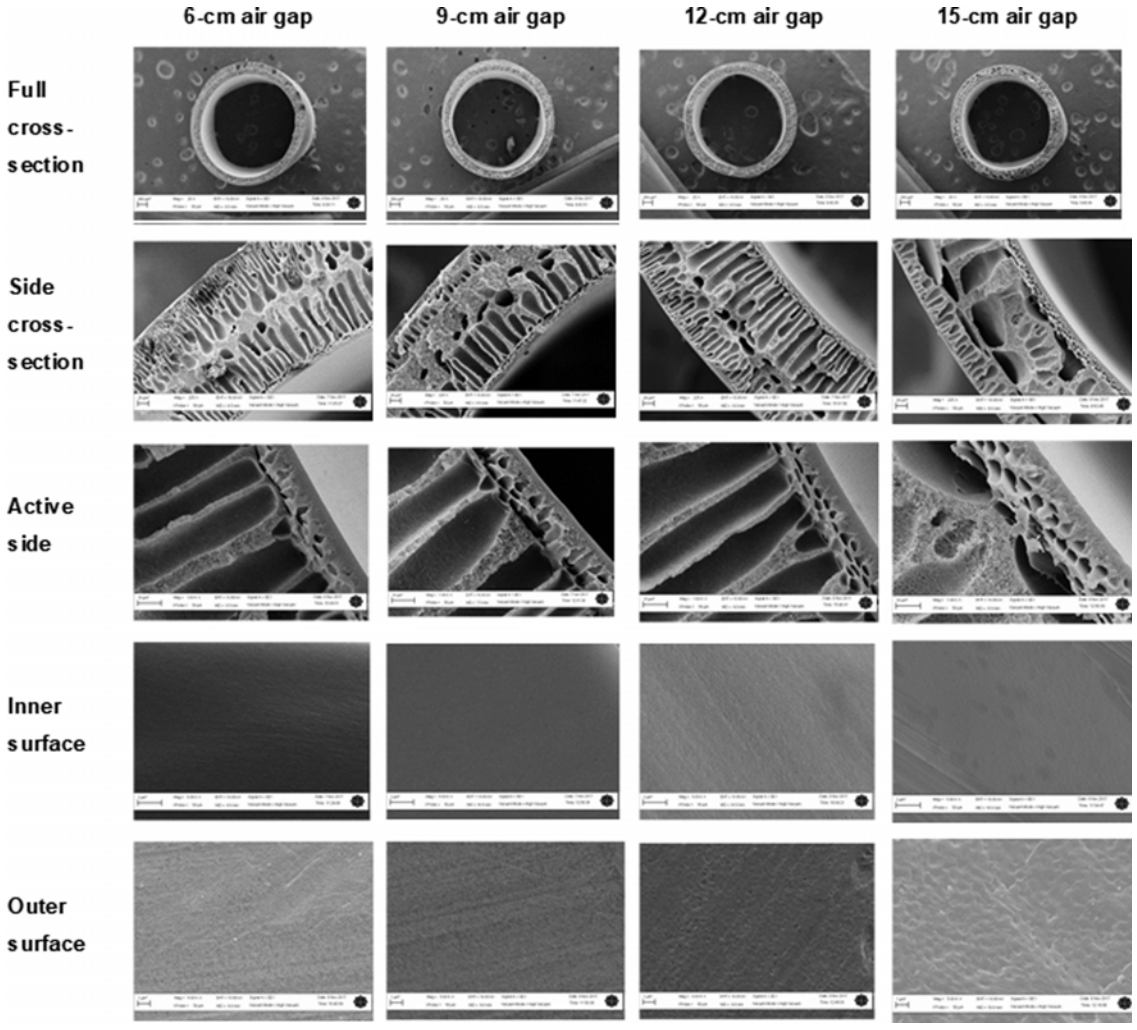

Fig. 2. SEM images of hollow fiber membrane substrate prepared at different air gap lengths.

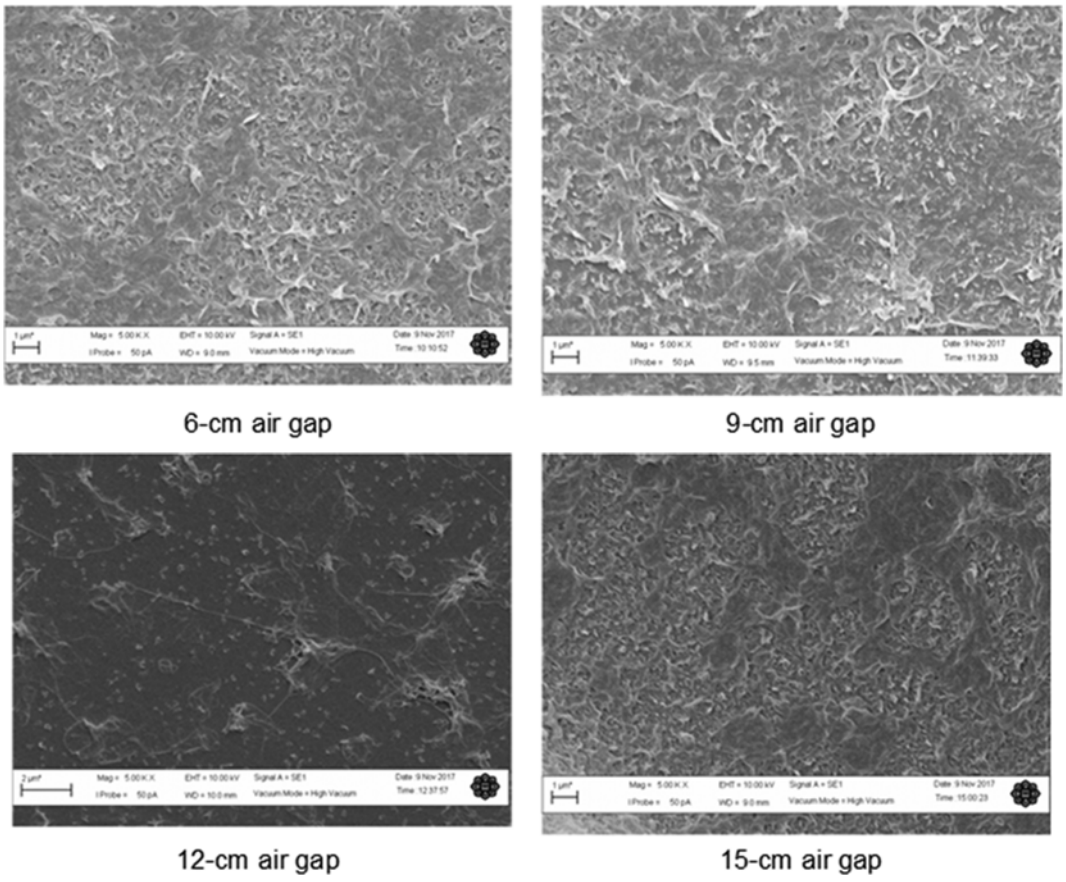

Fig. 3. SEM images of MPD thin film composite membrane formed using different membrane substrate (under magnification of 10,000×).

surface being immediately in contact with the bore fluid once the dope polymer left the spinneret [19]. The macrovoid structure changed from finger-like to the sponge-like structure as the air gap increased. Similar trends of membrane morphology were observed by Said et al. [12].

As the air gap increased, the contact time of the spun fiber with the bore fluid enhanced, thus increasing the inner macrovoid size [7]. Meanwhile, the sponge structure near the outer layer became looser with the increase of the air gap, which was coherent with the findings from Tang et al. [9]. The surface of the inner and outer membrane was smooth and dense without any visible pores under a magnification of 10,000×.

The effects of air gap distance on the diameter and wall thickness of the hollow fiber membrane are presented in Table 1. Both the inner and outer diameters of the membrane substrate diameters had decreased as the air gap length increased from 6 cm to 15 cm. Consequently, the wall thickness of the membrane was also reduced from 0.23 mm to 0.20 mm. The significant decrease in OD, ID and wall thickness of the membranes is due to the elongation of hollow fiber triggered by the gravity while traveling through the air gap. The fiber was stretched and became thinner, as reported previously by Korminouri et al. [7].

Table 1. Diameter and wall thickness of hollow fiber substrate membrane prepared at different air gap lengths

Air gap (cm)	6	9	12	15
OD (mm)	2.66	2.60	2.50	2.48
ID (mm)	2.20	2.16	2.08	2.08
Thickness (mm)	0.23	0.22	0.21	0.20

Fig. 3 shows the inner surface of the TFC membrane after the IP process. The inner surface of the membranes changed from a smooth surface, previously shown in the membrane substrate to the "leaf-like" folds surface. This indicated that a new, thin film was successfully formed on the membrane substrate after the IP. The ridge-and-valley structure is the typical morphology found in the MPD/TMC polyamide TFC membranes. The membrane substrate properties and polarity are the main caused for the morphology variation in the TFC membrane as shown in Fig. 3 because the IP condition remained constant in all of the membranes. The rate and extent of polymerization was controlled by the amount of MPD reaching to the reaction zone, and the extent to which the polyamide film formed in the pores [20]. The MPD aqueous solution would diffuse easily in the large pores compared to small pores. Fast penetration of the monomer solutions would lead to the thinning of the polyamide layers and high degree of defect on the top of the PSf membrane substrates [21]. Thus, the thickness and morphology of the polyamide active film formed on the membrane substrate would vary, depending on the pore size of the membrane substrate.

Table 2. Porosity and average pore size of membranes

Air gap (cm)	6	9	12	15
Porosity before IP, ε (%)	75.61±6.07	78.65±2.23	84.79±1.64	89.10±3.10
Porosity after IP, ε (%)	75.70±5.64	77.72±0.56	85.56±1.64	88.35±2.57
Average pore size, r_m before IP (nm)	4.46±0.56	5.58±0.53	9.25±0.22	8.82±1.14
Average pore size, r_m after IP (nm)	0.09±0.02	0.47±0.09	1.16±0.29	2.62±0.41

3. Porosity and Pore Size

The porosity and average pore size of the membrane substrate and TFC membranes are compiled in Table 2. The porosity of the membrane substrate increased as the air gap length increased from 6 cm to 12 cm; the membrane substrate spun at 6-cm air gap had the lowest porosity. This can be correlated with the membrane structure that had small and compact needle-like pores underneath the skin layer and less-occupied macrovoids at the middle structure, as seen in the cross-section of the membrane shown previously in Fig. 2. Meanwhile, the porosity of the TFC membrane after the IP did not change significantly compared to the membrane substrate's. The polyamide active layer formed after the IP was very thin and unable to penetrate across the whole membrane structure. As the porosity value is measured based on the portion of total void inside the membrane structure, it will not affect the overall porosity of the TFC membrane significantly.

In contrast to the porosity, the average pore size diameter of the membrane substrates increased with the increment of air gap lengths. At short air gap distance, rapid phase inversion without much chain relaxation had occurred, which resulted in small pore size membranes. Membrane substrates spun at the shortest air gap distance of 6 cm had the smallest mean pore diameter of 4.46±0.56 nm. As the air gap distance increased, die swell relaxation occurred. The stretch stress on the nascent membrane under the gravity produced numerous and larger pores, thus increasing the mean pore size [9]. As a result, the membrane substrate spun at 12 cm and 15 cm showed almost double the pore size diameter when compared to the 6-cm air gap. The average pore size of the TFC membranes was reduced drastically after the IP process. This reduction is due to the formation of active polyamide skin layer on the membrane substrates.

4. Filtration Performance

PWP of membrane substrate and TFC membranes are shown in Fig. 4. As the air gap increased from 6 cm to 15 cm, the PWP of the membrane substrate increased from 12.79±2.97 to 85.30±11.61 L/m^2·h·bar. This trend is correlated with the increase of the pore size of the membrane and MWCO, as the air gap increased, as discussed previously. The PWP for all PSf membrane substrates are within the UF membrane range, which is between 10 to 1,000 L/m^2·h·bar [22]. After IP, the PWP for all TFC membranes was reduced drastically, reaching the NF/RO range. This indicates that an active film layer was successfully formed at the lumen side of the hollow fiber after the IP. The PWP of the TFC membranes was in the range of 0.19±0.07 to 7.53±1.45 L/m^2·h·bar.

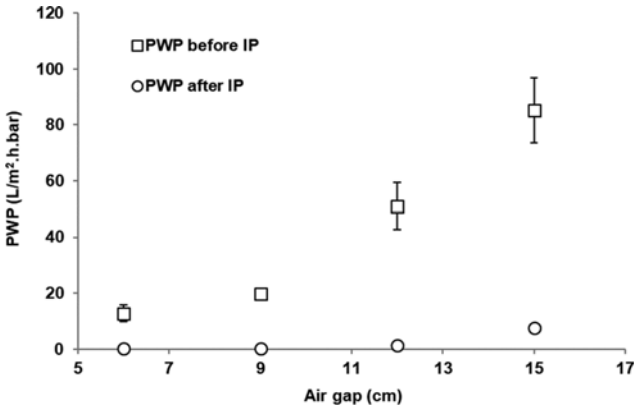

Fig. 4. Pure water permeability of the membranes before and after interfacial polymerization.

Table 3 shows the water and solute flux of TFC membranes measured at 3 bar. The water flux of the membrane substrate spun at 6 cm air gap recorded the lowest flux of 0.79±0.41 L/m^2·h·bar, while the substrate spun with the highest air gap of 15 cm recorded the highest flux of 21.60±6.59 L/m^2·h·bar. The trend of the flux change can be correlated with the value of the pore size of the membrane, as discussed previously.

During biomass processing in a biorefinery, sugars (mostly glucose and xylose) and other impurities such as acetic acid, furfural and hydroxymethyl furfural (HMF) are released after the hydrolysis process [23]. These sugars can be further concentrated or frac-

Table 3. Water and solute flux of TFC membrane measured at 3 bar

Properties	Air gap			
	6 cm	9 cm	12 cm	15 cm
Water flux before IP (L/m^2·h)	38.70±9.56	66.11±12.37	200.91±9.51	250.46±31.57
Water flux after IP (L/m^2·h)	0.79±0.41	0.51±0.19	3.76±1.76	21.60±6.59
Xylose flux (L/m^2·h)	0.41±0.27	0.27±0.20	2.48±1.86	25.92±14.32
Glucose flux (L/m^2·h)	0.62±0.18	0.39±0.29	2.27±1.59	33.88±23.87
Acetic acid flux (L/m^2·h)	0.84±0.26	0.48±0.25	2.56±1.08	28.08±18.30

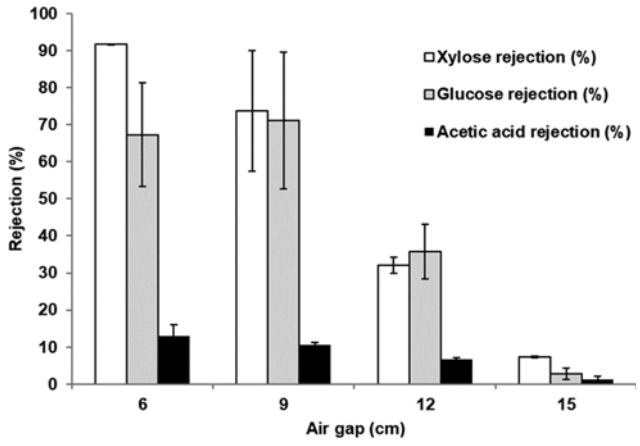

Fig. 5 Rejection of xylose, glucose and acetic acid using TFC membranes of different substrates.

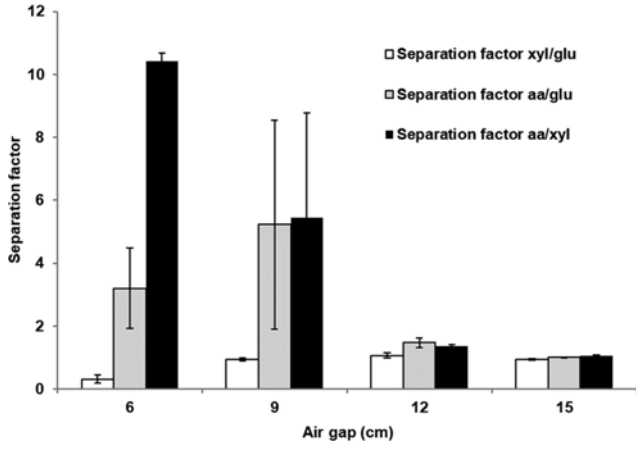

Fig. 6 Separation factor of xylose/glucose, acetic acid/glucose and acetic acid/xylose using TFC membranes of different substrates.

tionated to its individual component for converting to the specific product. Acetic acid that exists in the biomass hydrolysate needs to be removed because it can inhibit the microorganism growth during the sugar fermentation process later [24]. The TFC membrane solute rejection and separation factor are shown in Fig. 5 and Fig. 6, respectively. The properties of the TFC membranes are related directly to the properties of the membrane substrate because the IP process condition remain constant during membrane manufacturing. The TFC membrane having the substrate spun at 6 cm air gap exhibited a high solute rejection of 91.66±0.09% for xylose, 67.28±13.97 % for glucose, and 13.08±3.00% for acetic acid, which corresponds to the ideal separation factor of 3.20±1.27 for acetic acid/glucose and 10.42±0.25 for acetic acid/xylose. Meanwhile, the membrane having the substrate spun with the highest air gap of 15 cm exhibited the lowest solute rejection of 7.39±0.27% for xylose, 2.84±1.51% for glucose, and 1.37±0.72% for acetic acid, which resulted in the ideal separation factor of 1.01±0.01 for acetic acid/glucose and 1.07±0.01 for acetic acid/xylose.

Thicker and denser active layer was developed on the substrate surface with 6 cm air gap due to limit dispersion of polyamide into the small pores of the PSf substrate membrane. Ang et al. [25] observed a similar trend during the preparation of piperazine-based polyamide TFC NF membrane using PSf supports**.** On the other hand, in case of using membrane substrate spun at 15 cm air gap, the monomer solution can easily penetrate into the bigger pores, producing thin and less dense polyamide layers TFC membrane. Thin polyamide layers have higher chances of defect compared to the thick layer, which can lower the flux and solute rejection efficiency [26].

All the TFC hollow fiber membranes prepared in this study can be classified as NF and RO membranes based on their PWP values. The possible separation mechanism of the NF/RO TFC membrane could be attributed to the combination of the solution-diffusion, size exclusion, or Donnan effect transport mechanism [2]. For xylose and glucose, which are uncharged molecules, the solution-diffusion mechanism and size exclusion are the dominating transport mechanisms. It can be observed that the rejection of the uncharged solute correlates with the membrane pore size. The rejection of xylose was 91.66±0.09% and 7.39±0.27% at the pore size of 0.09 and 2.62 nm, respectively. As for acetic acid, which is a charged molecule, the filtration mechanism could be affected by the Donnan effect. The polyamide TFC hollow fiber is a negatively-charged membrane that is able to repel the acetic acid molecule, thereby increasing the acetic acid retention. However, in this study, the pH of the feed acetic acid was maintained at 2.71, which is below the acetic acid dissociation constant (pKa 4.756). Thus, the acetic acid molecules were in neutral form [2] and not significantly affected by the Donnan mechanism. The rejection of acetic acid still correlates with the membrane pore size as shown in Fig. 5, which means the separation is governed by solution-diffusion mechanism and size exclusion.

The separation factor of the TFC hollow fiber membrane prepared in this study was in the range of 0.31-1.07, 1.01-5.23 and 1.07-10.42 for xylose/glucose, acetic acid/glucose and acetic acid/xylose, respectively. The highest separation factor was observed in the separation of acetic acid from xylose. The separation factor was comparable to the commercial Desal-5 DK [27] and PA 400 Permeonics [28] membranes with the separation factor of 5.4 and 3.1, respectively. However, this value is extremely low compared to the Alfa Laval RO98pHt membrane which had an acetic acid/xylose separation factor of over 220 [2]. Nevertheless, further optimization on the filtration operating parameters could be done to improve the separation factor of the TFC hollow fiber membrane. Previously, Weng et al. [29] managed to increase the separation factor of Desal-5 DK membrane from 5.4 [27] to the 52 [29] by manipulating pH, temperature and pressure during the filtration process.

CONCLUSION

The membrane substrate MWCO can be easily manipulated by adjusting the air gap distance during the spinning process. Short air gap produces small MWCO membrane substrate compared to that of utilizing long air gap distance. The membrane substrate properties notably affect the overall performance of the TFC membrane. The best performance of the TFC membrane for the sepa-

ration of biomass hydrolysate components was produced using the membrane substrate prepared at 6 cm air gap distance. For biorefinery application, TFC hollow fiber membrane shows an advantage in terms of large surface area per unit volume, which is able to process a large amount of biomass hydrolysate solution. Furthermore, the TFC membrane prepared in this study was fine-tuned for the separation of specific solutes present in the biomass hydrolysate. Although the separation factor of the TFC hollow fiber membrane is acceptable, it is still low compared to that of the commercial membrane [2,30]. The identification of the dominant fabrication parameters and the interaction among the parameters remains for future study to improve the performance of the TFC hollow fiber membrane for biorefinery application.

FUNDING INFORMATION

The authors would like to thank the Ministry of Higher Education Malaysia and Universiti Malaysia Pahang for the financial support provided under the Fundamental Research Grant Scheme (RDU170117-FRGS/1/2017/TK02/UMP/02/8) and Research University Grant Scheme (UMP-RDU150316), respectively.

CONFLICT OF INTEREST

The authors declare that they have no conflicts of interest.

REFERENCES

1. N. Nguyen, C. Fargues, W. Guiga and M.-L. Lameloise, *J. Membr. Sci.*, **487**, 40 (2015).
2. F. Zhou, C. Wang and J. Wei, *J. Membr. Sci.*, **429**, 243 (2013).
3. W. Fang, L. Shi and R. Wang, *J. Membr. Sci.*, **468**, 52 (2014).
4. D. Wu, Y. Huang, S. Yu, D. Lawless and X. Feng, *J. Membr. Sci.*, **472**, 141 (2014).
5. N. Misdan, W. J. Lau, A. F. Ismail and T. Matsuura, *Desalination*, **329**, 9 (2013).
6. S. Zhu, S. Zhao, Z. Wang, X. Tian, M. Shi, J. Wang and S. Wang, *J. Membr. Sci.*, **493**, 263 (2015).
7. F. Korminouri, M. Rahbari-Sisakht, D. Rana, T. Matsuura and A. F. Ismail, *Sep. Purif. Technol.*, **132**, 601 (2014).
8. M. Radjabian, J. Koll, K. Buhr, U. A. Handge and V. Abetz, *Polym. (United Kingdom)*, **54**, 1803 (2013).
9. Y. Tang, N. Li, A. Liu, S. Ding, C. Yi and H. Liu, *Desalination*, **287**, 326 (2012).
10. T. Liu, D. Zhang, S. Xu and S. Sourirajan, *Sep. Sci. Technol.*, **27**, 161 (1992).
11. M. Khayet, *Chem. Eng. Sci.*, **58**, 3091 (2003).
12. N. Said, H. Hasbullah, A. F. Ismail, M. Nidzhom, Z. Abidin, P. Sean and M. H. Dzarfan, *Chem. Eng. Trans.*, **56**, 1591 (2017).
13. T. S. Chung, Z. L. Xu and W. Lin, *J. Appl. Polym. Sci.*, **72**, 379 (1999).
14. S. K. Maurya, K. Parashuram, P. S. Singh, P. Ray and A. V. R. Reddy, *Desalination*, **304**, 11 (2012).
15. D. Li, R. Wang and T.-S. Chung, *Sep. Purif. Technol.*, **40**, 15 (2004).
16. G. L. Miller, *Anal. Chem.*, **31**, 426 (1959).
17. E. Anuar, S. M. Saufi, M. N. A. Seman, H. W. Yussof and A. F. Ismail, *Chem. Eng. Trans.*, **56**, 1099 (2017).
18. I. I. Yusoff, R. Rohani and A. W. Mohammad, *Malaysian J. Anal. Sci.*, **21**, 484 (2017).
19. Z. L. Cheng, X. Li, Y. Da Liu and T. S. Chung, *J. Membr. Sci.*, **506**, 119 (2016).
20. I. M. A. ElSherbiny, R. Ghannam, A. S. G. Khalil and M. Ulbricht, *J. Membr. Sci.*, **493**, 782 (2015).
21. M. Fathizadeh, A. Aroujalian and A. Raisi, *Desalination*, **284**, 32 (2012).
22. B. Van der Bruggen, C. Vandecasteele, T. Van Gestel, W. Doyen and R. Leysen, *Environ. Prog.*, **22**, 47 (2003).
23. D. L. Grzenia, D. J. Schell and S. R. Wickramasinghe, *J. Membr. Sci.*, **322**, 189 (2008).
24. G.-L. Guo, W.-H. Chen, W.-H. Chen, L.-C. Men and W.-S. Hwang, *Bioresour. Technol.*, **99**, 6046 (2008).
25. M. Ang, V. Lau, Y.-L. Ji, S.-H. Huang, Q. An, A. Caparanga, H.-A. Tsai, W. Hung, C.-C. Hu, K.-R. Lee and J.-Y. Lai, *Polymers (Basel)*, **9**, 505 (2017).
26. J. Li, M. Wei and Y. Wang, *Chinese J. Chem. Eng.*, **25**, 1676 (2017).
27. Y.-H. Weng, H.-J. Wei, T.-Y. Tsai, W.-H. Chen, T.-Y. Wei, W.-S. Hwang, C.-P. Wang and C.-P. Huang, *Sep. Purif. Technol.*, **67**, 95 (2009).
28. S. K. Maiti, Y. Lukka Thuyavan, S. Singh, H. S. Oberoi and G. P. Agarwal, *Bioresour. Technol.*, **114**, 419 (2012).
29. Y.-H. Weng, H.-J. Wei, T.-Y. Tsai, T.-H. Lin, T.-Y. Wei, G.-L. Guo and C.-P. Huang, *Bioresour. Technol.*, **101**, 4889 (2010).
30. F. Zhou, C. Wang and J. Wei, *Bioresour. Technol.*, **131**, 349 (2013).